ELSEVIER

Ion escape at Mars: Comparison of a 3-D hybrid simulation with Mars Express IMA/ASPERA-3 measurements

E. Kallio [a,*], A. Fedorov [b], E. Budnik [b], T. Säles [a], P. Janhunen [a], W. Schmidt [a], H. Koskinen [a,q],
P. Riihelä [a], S. Barabash [c], R. Lundin [c], M. Holmström [c], H. Gunell [c], K. Brinkfeldt [c], Y. Futaana [c],
H. Andersson [c], M. Yamauchi [c], A. Grigoriev [c], J.-A. Sauvaud [b], J.-J. Thocaven [b], J.D. Winningham [d],
R.A. Frahm [d], J.R. Sharber [d], J.R. Scherrer [d], A.J. Coates [e], D.R. Linder [e], D.O. Kataria [e], J. Kozyra [f],
J.G. Luhmann [g], E. Roelof [h], D. Williams [h], S. Livi [h], C.C. Curtis [i], K.C. Hsieh [i], B.R. Sandel [i],
M. Grande [j], M. Carter [j], S. McKenna-Lawler [k], S. Orsini [l], R. Cerulli-Irelli [l], M. Maggi [l], P. Wurz [m],
P. Bochsler [m], N. Krupp [n], J. Woch [n], M. Fränz [n], K. Asamura [o], C. Dierker [p]

[a] Space Research Unit, Finnish Meteorological Institute, Erik Palménin aukio 1, P.O. Box 503, FIN-00101 Helsinki, Finland
[b] Centre d'Etude Spatiale des Rayonnements, BP-4346, F-31028 Toulouse, France
[c] Swedish Institute of Space Physics, Box 812, S-98 128, Kiruna, Sweden
[d] Southwest Research Institute, San Antonio, TX 7228-0510, USA
[e] Mullard Space Science Laboratory, University College London, Surrey RH5 6NT, UK
[f] Space Physics Research Laboratory, University of Michigan, Ann Arbor, MI 48109-2143, USA
[g] Space Science Laboratory, University of California in Berkeley, Berkeley, CA 94720-7450, USA
[h] Applied Physics Laboratory, Johns Hopkins University, Laurel, MD 20723-6099, USA
[i] University of Arizona, Tucson, AZ 85721, USA
[j] Rutherford Appleton Laboratory, Chilton, Didcot, Oxfordshire OX11 0QX, UK
[k] Space Technology Ltd., National University of Ireland, Maynooth, Co. Kildare, Ireland
[l] Istituto di Fisica dello Spazio Interplanetari, I-00133 Rome, Italy
[m] Physikalisches Institut, University of Bern, CH-3012 Bern, Switzerland
[n] Max-Planck-Institut für Aeronomie, D-37191 Katlenburg-Lindau, German
[o] Institute of Space and Astronautical Science, 3-1-1 Yoshinodai, Sagamichara, Japan
[p] Technical University of Braunschweig, Hans-Sommer-Strasse 66, D-38106 Braunschweig, Germany
[q] Department of Physical Sciences, University of Helsinki, P.O. Box 64, FIN-00014 Helsinki, Finland

Abstract

We have analysed ion escape at Mars by comparing ASPERA-3/Mars Express ion measurements and a 3-D quasi-neutral hybrid model. As Mars Express does not have a magnetometer onboard, the analysed IMA data are from an orbit when the IMF clock angle was possible to determine from the magnetic field measurements of Mars Global Surveyor. We found that fast escaping planetary ions were observed at the place which, according to the 3-D model, is anticipated to contain accelerated heavy ions originating from the martian ionosphere. The direction of the interplanetary magnetic field was found to affect noticeably which regions can be magnetically connected to Mars Express and to the overall 3-D Mars–solar wind interaction.
© 2005 Elsevier Inc. All rights reserved.

Keywords: Mars, atmosphere; Ionospheres

---

* Corresponding author. Fax: +358 9 1929 4603.
   E-mail address: esa.kallio@fmi.fi (E. Kallio).

1. Introduction

Mars provides an object for studying the effects of direct solar wind–planetary atmosphere interaction because it does not have a notable global intrinsic magnetic field that could protect it against the direct impact with the solar wind particles. This direct interaction may have some cosmogonical importance for the evolution of martian atmosphere because the solar wind accelerates ionised planetary neutrals resulting in atmospheric loss (Lundin et al., 1990).

Developing a detailed model to interpret the properties of the escaping ions is a challenging problem because it should model multiion species plasma, take into account the finite gyroradius effects of the ions and contain three-dimensional (3-D) ion velocity distribution functions. A 3-D multifluid magnetohydrodynamic model provides a self-consistent approach to study plasma physical processes near Mars with high, a few-kilometre-size (Ma et al., 2004), spatial resolution. A quasi-neutral hybrid model, QNH, a self-consistent approach where ions are particles while electrons form a massless charge-neutralising fluid. The QNH model takes into account kinetic effects and the approach has been used to study the properties of the plasma and the magnetic field near Mars (Brecht and Ferrante, 1991; Shimazu, 1999; Kallio and Janhunen, 2002).

The first direct measurements of the escaping martian ions were performed by two ion mass spectrometers, ASPERA and TAUS instruments, on Phobos-2 mission in early 1989. Based on the ASPERA/Phobos-2 measurements the total atomic oxygen ion (O^+) loss rate was estimated to be about 2×10^{25} s^{-1} and the total atomic and molecular oxygen ion loss rate about $1 \, kg \, s^{-1}$ (Lundin et al., 1990). The latest and the most comprehensive in situ measurements of the escaping planetary ions come from the ASPERA-3 instrument onboard Mars Express (MEX) by its IMA (Ion Mass Analyser) detector. IMA has observed heavy planetary ions near the planet on the dayside (Lundin et al., 2004) and escaping planetary ions on the nightside (Fedorov et al., 2006). In this paper we analyse an orbit of MEX when escaping ions were observed on the nightside near the terminator plane at a time when the direction of the interplanetary magnetic field, IMF, was possible to derive from the magnetic field measurements of the Mars Global Surveyor (MGS). We study the event using a 3-D three ion species QNH model version that contains H^+, O^+, and O_2^+ ions and enables us to analyse how the properties of the escaping ions are related to the morphology of the magnetic field.

In this paper, we first present IMA data from the chosen orbit. Then we describe the 3-D QNH model and show the properties of the solar wind, escaping planetary ions and the morphology of the magnetic field near Mars. Finally, the 3-D nature of the Mars–solar wind interaction is discussed.

2. Observations: Orbit 555

IMA provides ion measurements in the energy range 0.02–30 keV/q for the main ion components H^+, H_2^+, He^+, O^+ and the group of molecular ions ($20 < amu \, e^{-1} < {\sim}80$). The instrument has a $4.6° \times 360°$ field of view with electrostatic

sweeping performing elevation ($\pm45°$) coverage (see Barabash et al., 2004, for the details of IMA instrument).

Fig. 1a shows the position of MEX at the analysed Orbit 555 on June 27, 2004 at 03:00–03:35 UT. The ion measurements were near the terminator plane on the nightside as the spacecraft approached Mars. At first IMA observed light ions at m/q (mass per charge ratio) of 1.5–3 amu e^{-1} but no heavy ($m/q = 12$–40 amu e^{-1}) ions were detected (Fig. 1b) between 03:00 and 03:16 UT. Although the electrostatic elevation deflection scans versus time cause modulation of the data, Fig. 1 shows that the countrate and the energy of the light ions decreased when MEX came closer to Mars. At about 03:17 UT, heavy ions were observed at the energy of ${\sim}2$ keV. Then the energy and the countrate of heavy ions decreased from 03:17 to 03:35 UT.

IMA energy–mass spectrogram collected between 03:18-03:20 UT is shown in Fig. 1c. Even though IMA was in a data collection mode dedicated to the study of planetary ions, it was not able to detect H^+ ions in detail because the instruments' low-energy cut-off limit exceeded the solar wind H^+ energy. Solar wind alpha particles (He^{2+}) can, however, be identified because its low-energy cut-off limit is slightly lower than the He^{2+} energy. The energy–mass matrix shows that the measured plasma contains ions whose m/q ratio corresponds to m/q ratios of O^+ ($m/q = 16$) and O_2^+ ($m/q = 32$) ions. Note that the mass resolution of IMA is not good enough to distinguish O^+ from C^+, and O_2^+ from CO^+.

A comparison between a QNH model and ASPERA/Phobos-2 planetary ion observations from 1989 indicated the importance of the direction of the IMF (Kallio and Janhunen, 2002). The direction of the interplanetary magnetic field, $\mathbf{B}_{sw}$, controls the direction of the convective electric field, $\mathbf{E}_{sw}$ ($= -\mathbf{U}_{sw} \times \mathbf{B}_{sw}$, where $\mathbf{U}_{sw}$ is the velocity of the solar wind). In a QNH model the velocity of planetary ions is higher on the so-called $+E_{sw}$ hemisphere than on the $-E_{sw}$ hemisphere. Here the $+E_{sw}$ ($-E_{sw}$) hemisphere refers to the hemisphere on which $\mathbf{E}_{sw}$ points away from (toward) the plane of the Mars–Sun line and the IMF. The density of the planetary ions are, on the contrary, higher on the $-E_{sw}$ hemisphere than on the $+E_{sw}$ hemisphere.

Orbit 555 was chosen for to this paper because of the availability of MGS magnetic field data to determine the IMF clock angle during the IMA observations. The IMF clock angle is defined as the angle of the vector $(0, B_y, B_z)$ from the y-axis, where B_y and B_z are the IMF y and z components in the MSO coordinate system: x points from Mars to the Sun, y points opposite to the orbital motion of Mars and z completes the right hand coordinate system. The IMF piles up against Mars and drapes around the planet, making possible the determination of the IMF clock angle from MGS B_y and B_z measurements outside of the martian crustal magnetic field (see Fedorov et al., 2006, for the details of the determination of the IMF clock angle). The absolute values of B_y and B_z cannot be determined by this method, neither the total magnitude of IMF.

The directions of the IMF and $\mathbf{E}_{sw}$ on the Orbit 555 are given in Fig. 2 in addition to the position of MEX. IMF clock angle was about 300°. As seen in Fig. 2, the orbit of MEX was in
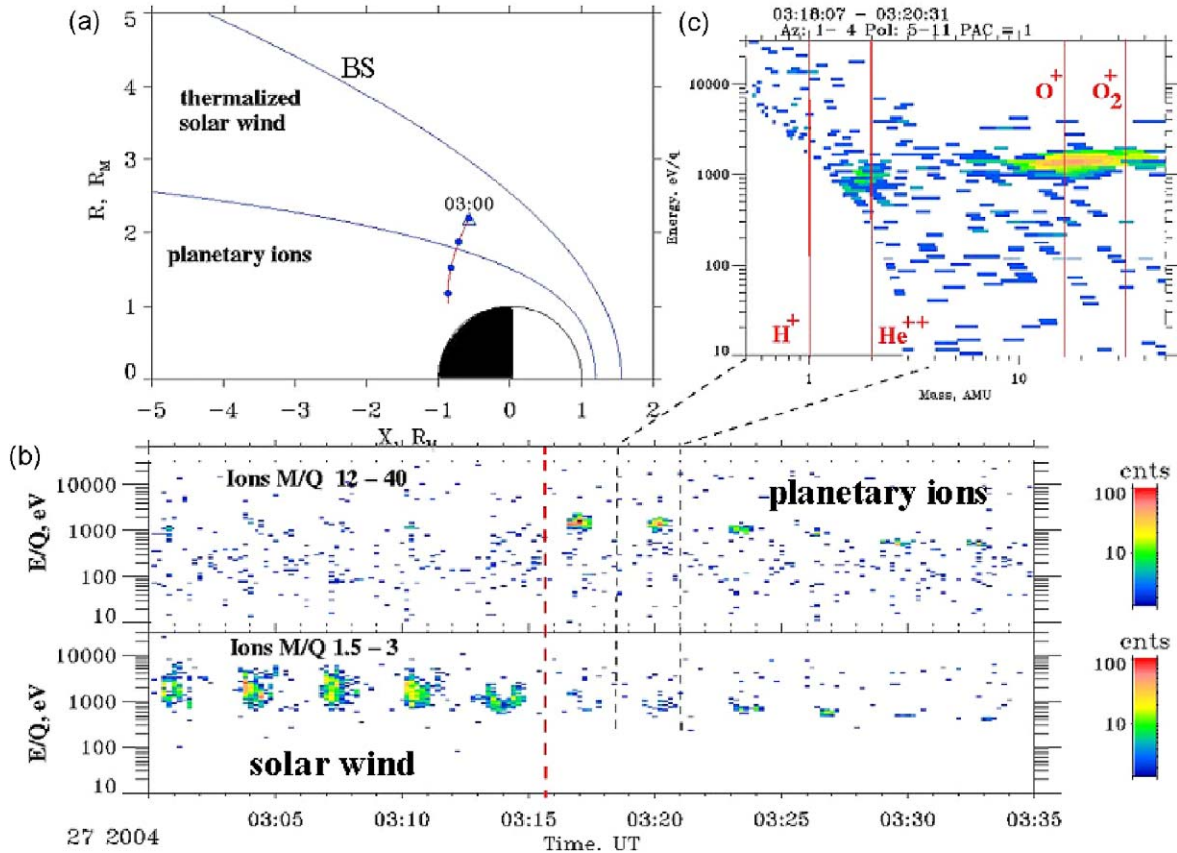
Fig. 1. (a) The position of Mars Express on June 27, 2004, on 03:00–03:30 UT (Orbit 555) in MSO coordinates. The space craft positions are shown by dots at 10-min time intervals. Two solid curves show a typical position of the bow shock (BS) and the region where ASPERA/Phobos-2 in 1989 observed a sudden decrease in the flux of the solar wind protons. (b) IMA/ASPERA-3 heavy ion (upper panel) and light ion (lower panel) observations on June 27, 2004, between 03:00 to 03:35 UT. (c) IMA mass–energy matrix from 03:18:07–03:20:31 UT.
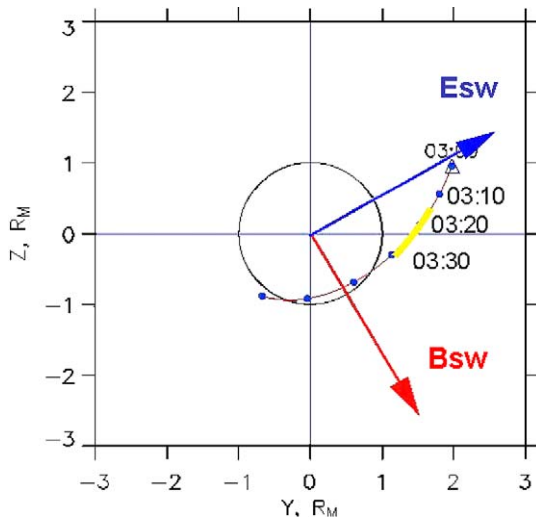

Fig. 2. The direction of the IMF, $\mathbf{B}_{sw}$, on the yz plane derived from Mars Global Surveyor magnetic field observations on June 27, 2004 and the direction of the convective electric field $\mathbf{E}_{sw}$ ($= -\mathbf{U}_{sw} \times \mathbf{B}_{sw}$). The solid lines show the orbit of MEX on June 27, 2004, at 03:00–04:00 UT.

the region where $\mathbf{E}_{sw}$ is pointing away from Mars (the $+E_{sw}$ hemisphere), that is, on the hemisphere where highly accelerated planetary ions can be found in a QNH model, as will be seen in the next section.

3. The QNH model

The description of the 3-D QNH model can be found in our previous publications (see Kallio and Janhunen, 2002) and here we list only some basic features which are of importance for the present study.

The size of the simulation box is $-5.3\,R_M < x < 3.2\,R_M$; $-4.2\,R_M < y, z < 4.2\,R_M$ ($R_M = 3393$ km = the radius of Mars) in MSO coordinates (Fig. 3). The simulation contains three grid sizes, 720 km ($\sim 0.2\,R_M$), 360 km ($\sim 0.1\,R_M$), and 180 km ($\sim 0.05\,R_M$). The grid is refined only on the dayside in order to avoid the possibility that grid refinement may result in artificial changes of the parameters in the analysed region on the nightside. The obstacle in the simulation box is a sphere of radius $r = r_{obstacle} = 3600$ km. An ion is removed from the simulation if it moves inside the obstacle or out of the simulation box. The total number of ions in the simulation is ~ 2.5 million, the average number of particles per a cell is 20, and the time step, dt, is 0.04 s. The values of the solar wind density (n_{sw}) and velocity (U_{sw}) are not know and in this paper their values were artificially chosen to be 3 cm^{-3} and $[-450, 0, 0]$ km s^{-1}, respectively. The interplanetary magnetic field (B_{sw}) was taken to be $[\cos(55°), -\sin(55°), 0] \times 1.12$ nT $= [0.64, -0.92, 0]$ nT, respectively. The angle 55° is a theoretical value of the garden hose angle of the IMF field line at Mars position calculated for
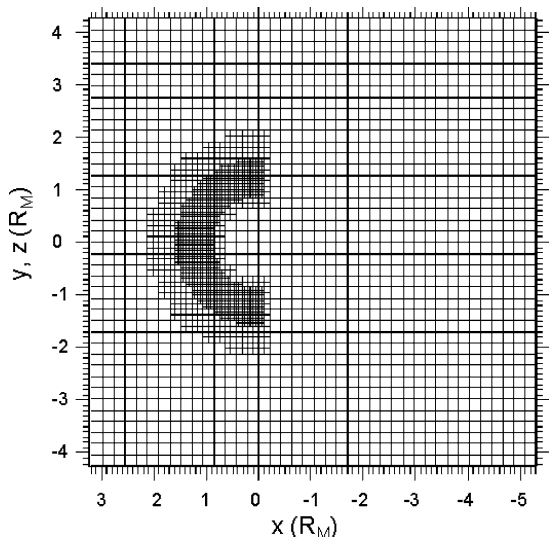
Fig. 3. The structure of the grid on the xy and xz planes. Grid refinement was used to produce two refined spherical half spheres on the dayside.

the average solar wind conditions. Note that B_x and $|\mathbf{B}_{sw}|$ have not been determined from MGS data, and that the solution can also be applied to other IMF clock angles than $300°$ by rotating the solution, or the orbit of MEX, around the x-axis. Finally, the model does not contain the recently observed (Acuña et al., 1998) martian crustal magnetic field.

In the hybrid model ions are treated as particles accelerated by the Lorentz force. The model contains three ion species, H^+, O^+, and O_2^+ ions. These ions have three sources. The protons are mainly solar wind protons launched into the simulation box at the front face. Protons were also generated from a hydrogen corona of the scale height of 2.61×10^4 km (from Barabash et al., 2002, Table 1) but with a low total ion production rate 1.8×10^{24} s^{-1}. In this study we do not distinguish solar wind protons from the protons originating from the neutral hydrogen corona.

Oxygen ions are produced from two sources: (1) from the neutral exosphere with a probability directly proportional to the neutral density and (2) from the obstacle boundary that mimics the exopause. The neutral scale height was 1.78×10^4 km (from Barabash et al., 2002, Table 1). The molecular oxygen ions were emitted from the obstacle boundary without a neutral exosphere. The total ion production rates from the neutral corona, q_{corona}, and the total ion emission rate from the obstacle boundary, q_{iono}, were chosen to be $q_{corona}(O^+) = 2.7 \times 10^{23}$ s^{-1}, $q_{iono}(O^+) = 1.4 \times 10^{25}$ s^{-1}, and $q_{iono}(O_2^+) = 2 \times 10^{25}$ s^{-1}. Our previous comparisons between ASPERA/Phobos-2 ions measurements and the QNH model have indicated that the determination of the value of the most appropriate total ion production and emission rates is a problem that cannot be solved self-consistently in the used QNH model. The largest limitation is that the QNH model does not contain self-consistently derived ionosphere and, therefore, the total emission rate is a free parameter in the model. For example, the emission rates are not equal with the total ion loss rates because the emitted ions can return to the obstacle. Nevertheless, the total ion emission rate of $\sim 2 \times 10^{25}$ s^{-1} was found to reproduce relatively well the

plasma and magnetic field measurements from Phobos-2 circular orbits (Kallio and Janhunen, 2002). A more detailed fine tuning of the ion source rates is possible when the ion density estimates based on IMA data become available.

Fig. 4 gives the particle density of H^+, O^+, and O_2^+ based on the QNH model. The density of protons increases at the bow shock and it becomes less than the density of the solar wind behind the planet. A line is included to show a typical position of the conical bow shock (from Slavin et al., 1991: $e = 1.02$, $L = 2.04$ R_M, and $xo = 0.55$ R_M). A black line between the bow shock and Mars represents a region where the flux of the solar wind protons was found to decrease substantially according to ASPERA/Phobos-2 ion measurements in 1989 (from Kallio, 1996). A notable feature in $n(O_2^+)$ is that while the x component of the IMF causes only a slight dawn–dusk asymmetry there exists a substantial $+E_{sw}$ hemisphere $(z < 0)/-E_{sw}$ hemisphere $(z > 0)$ asymmetry caused by the convective electric field. The convective electric field accelerated O_2^+ to the $-z$ direction causing a smooth transition layer on the $z < 0$ hemisphere filled with escaping planetary ions. The same is true for the O^+ population which was emitted from the obstacle boundary. Note that $n(O^+)$ does not vary smoothly in the solar wind and in the magnetosheath because of the small number of O^+ emitted from the exosphere into the simulation box.

In Fig. 5 the spatial asymmetry is shown in more detail by showing the density of the planetary ions on the $x = -0.5$ R_M plane which is close to the site of the analysed IMA observations come from. A clear asymmetry exists on $n(O_2^+)$ with respect to the direction of $\mathbf{E}_{sw}$. The maximum density is located near Mars on the $-E_{sw}$ $(z > 0)$ hemisphere because the convective electric field pushes the planetary ions toward Mars while on the $+E_{sw}$ $(z < 0)$ hemisphere the planetary ions are accelerated away from Mars. The low density values at $+E_{sw}$ $(z < 0)$ on the xz-plane may be a result of a strong convective electric field or a "slingshot" effect, as will be discussed later. The density asymmetry is not so clearly seen on $n(O^+)$ because O^+ originate also from the neutral oxygen corona, which decreases density gradients. One can see that while MEX approached Mars on Orbit 555 it flew through a smooth transition layer on the $+E_{sw}$ $(z < 0)$ hemisphere. Note that, as mentioned before, the situation for other IMF clock angles can be obtained by rotating the orbit of MEX around the x-axis.

On the nightside a magnetotail is formed (Fig. 6a). Fig. 6b illustrates that the properties of the magnetic field at the site of the observations depend on the IMF clock angle. The piling up of the magnetic field lines increases the magnitude of the magnetic field at the $x = -0.5$ R_M plane near the site of the analysed IMA observations.

Fig. 7 illustrates the morphology of the magnetic field in the QNH model. The magnetic field lines were derived by choosing 30 starting points along a straight line between the points $(-0.5, 0, 1)$ R_M and $(-0.5, 0, 3)$ R_M in order to study how the region from which IMA data come is magnetically connected to different plasma regions near Mars. Two different magnetic field line types can be identified. First, highly draped field lines connected to the starting points close to the planet. In 3-D view (Fig. 7a) these magnetic field lines form magnetic tail lobes in
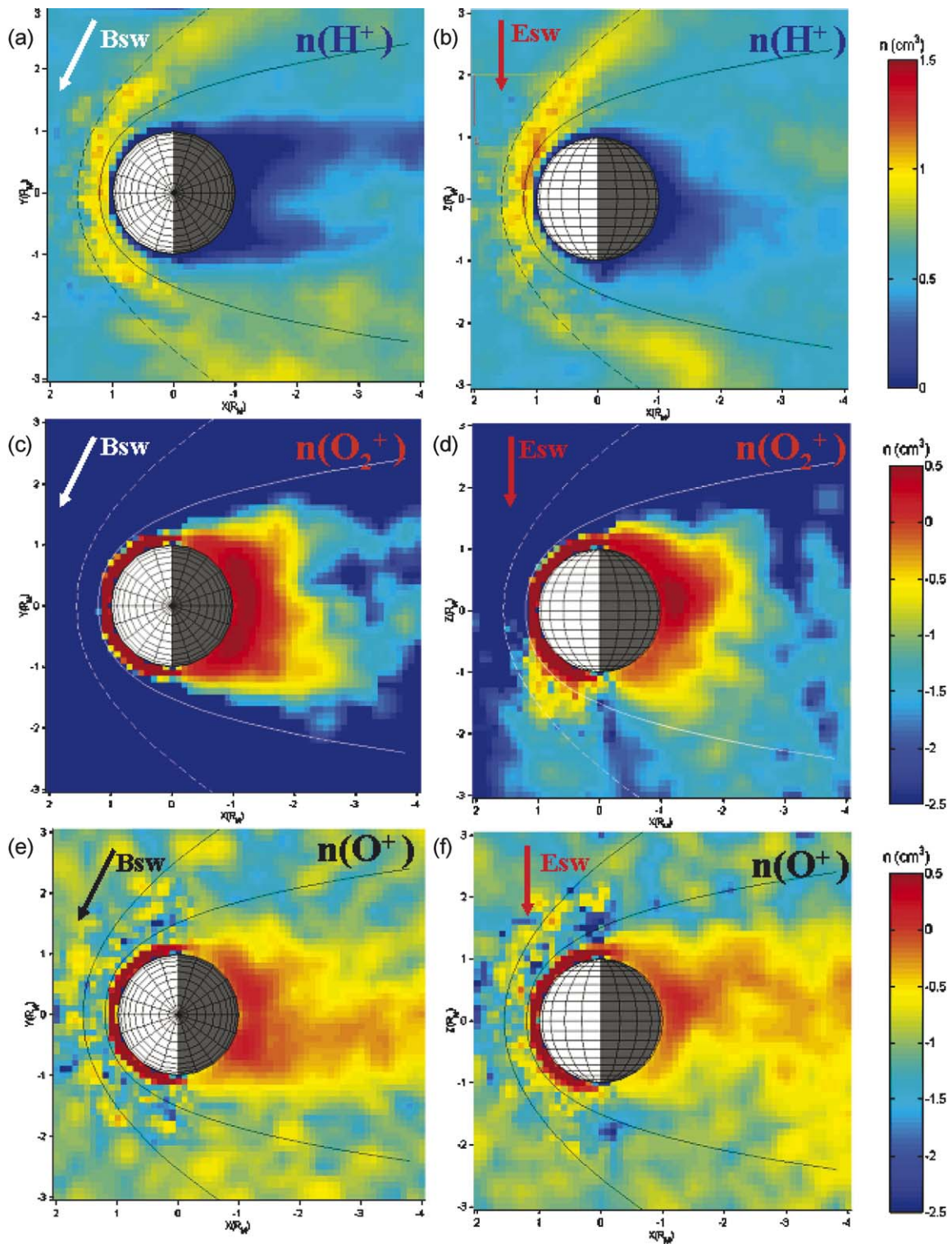
Fig. 4. The particle density [cm^{-3}] of (a, b) protons, (c, d) oxygen ions, and (e, f) molecular oxygen ions on the XY and XZ planes based on the QNH model. The direction of the interplanetary magnetic field, $\mathbf{B}_{sw}$ ($= [\cos(55°), -\sin(55°), 0] \times 1.12$ nT), and the convective electric field, $\mathbf{E}_{sw}$ ($= [0, 0, -|\mathbf{E}_{sw}|]$), are shown by arrows. Note that the viewpoint in (a), (c), and (e) is on the $-z$ hemisphere. See text for details.

the $z > 0$ hemisphere. Note also how the magnetic field lines seem to "slip" around the point $(0, 0, 1)$ R_M, sometimes called as the "magnetic pole." These highly draped field lines can be associated with a strong $\mathbf{j} \times \mathbf{B}$ force that acts as a "slingshot" accelerating planetary ions away from the planet. Second, only

moderately draped magnetic field lines are associated with the starting points far away from Mars. If MEX could have been moved toward Mars along a straight line, it would have moved from a magnetosheath-like magnetic field to the magnetotail-like magnetic field.
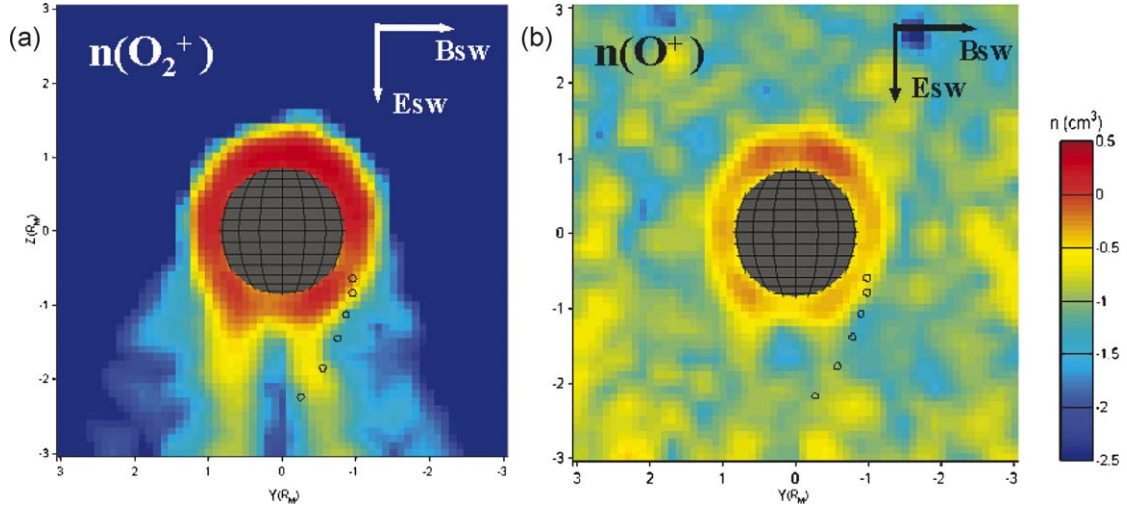
Fig. 5. (a) The density of O_2^+ ions and (b) the density of O^+ ions on the $x = -0.5$ R_M plane according to the QNH model. The view is from the tail toward Mars. Six black circles are included to show the path of MEX on June 27, 2004 at 03:00–03:35 UT. Note that the orbit of MEX is rotated around the x-axis so that the IMF component perpendicular to the x-axis points to the $-y$ direction.
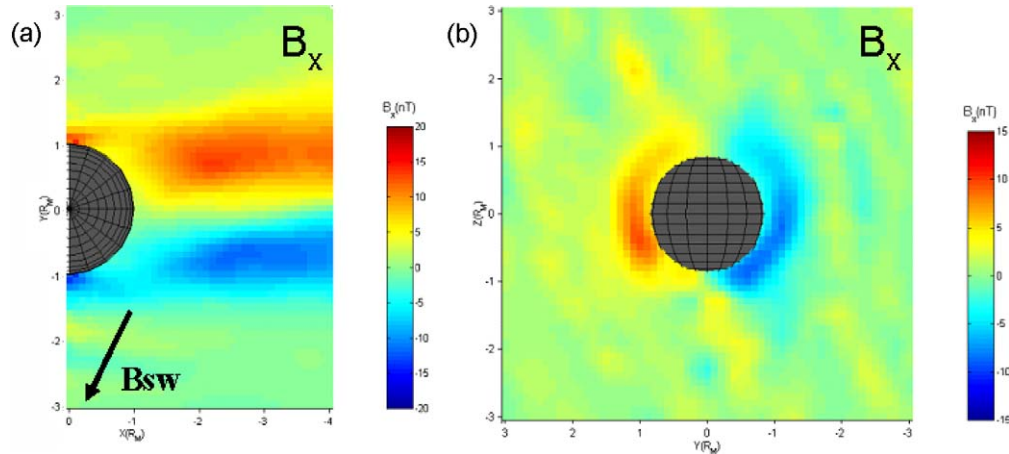

Fig. 6. The x component of the magnetic field (a) on the nightside on the xy plane and (b) on the $x = -0.5$ R_M plane based on the QNH model.

In reality spacecraft do not move along straight lines, which results in more complicated magnetic field draping patters than shown in Fig. 7. Figs. 8a–8d give the magnetic field lines calculated using the orbit of MEX on June 27, 2004 at 03:00–03:35 UT and the observed IMF clock angle. In Figs. 8a–8d the orbit of MEX and the magnetic field lines were rotated 120° clockwise around the x-axis to point the IMF to the $-y$ direction in order to help the eye to catch the draping of the magnetic field lines more clearly. The draping pattern is similar to the one seen in Fig. 7 with the modifications caused by the fact that now all three coordinates of the starting points of the field line tracing vary from point to point along the orbit of MEX. The simulation suggests that MEX flew from a moderately draped magnetic field line region (the magnetosheath) to a severely draped magnetic field line region (the magnetotail).

Figs. 8e–8h show the magnetic field draping for the IMF clock angle of 180° that was used in the QNH model. In this case MEX would have remained nearer the XY plane than in the 120° clock angle case (Figs. 8a–8d). Consequently, MEX would never have come to a highly draped magnetotail field line

region. Note also how the magnetic field lines are now draped around Mars far on the dayside. In the Orbit 555 case (Figs. 8a–8d) the magnetic field lines remain mostly on the nightside extending only slightly on the dayside around the "magnetic pole."

4. Comparison: IMA data vs QNH model

A comparison between IMA energy spectra data, and the plasma and the magnetic field derived along the orbit of MEX are given in Fig. 9. Determination of the macroscopic parameters from the shown IMA measurements is still in progress and we cannot yet perform a detailed data–model comparison. Nevertheless, certain similarities can already be seen. In the hybrid model the velocities of the heavy ions (O^+, O_2^+) and the light ions (H^+) decrease with time much as observed by IMA. At the same time, according to the QNH model, MEX is approaching the high density planetary ion region, as already seen in Fig. 5. Note also how the magnetic field x component changes its sign from the magnetosheath-like magnetic field ($B_x > 0$) to the
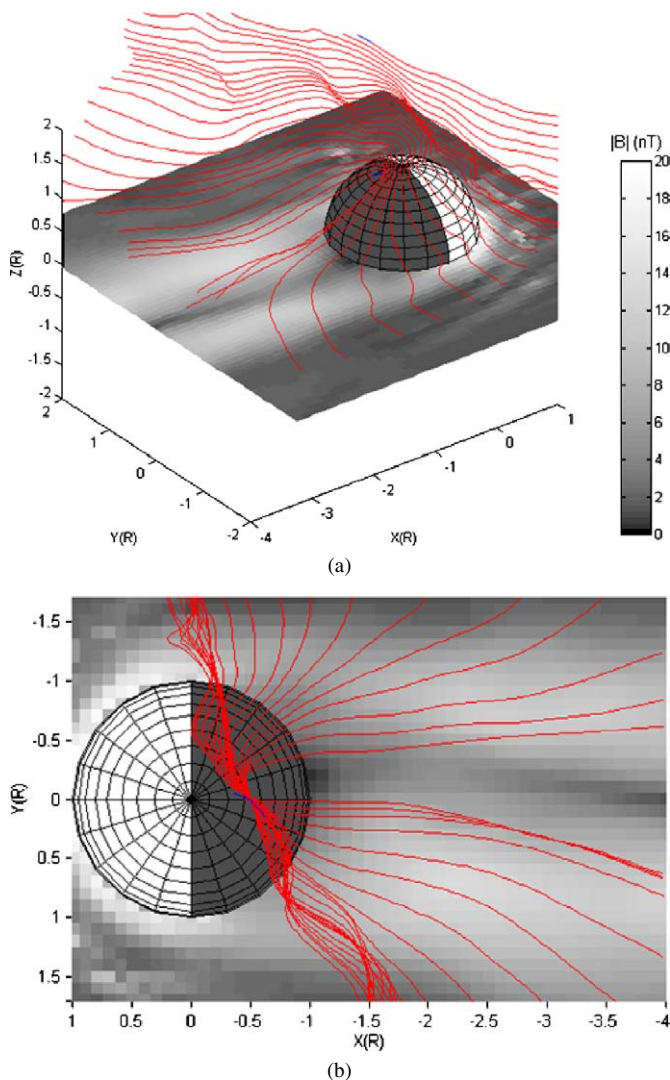
Fig. 7. An example of the magnetic field lines based on the QNH model: (a) 3-D view and (b) the same field lines now viewed from $z > 0$. The total magnetic field is shown on the xy plane by a grey colour scale.

magnetotail-like magnetic field ($B_x < 0$) about the same time when IMA starts to detect heavy planetary ions. Same changes of the direction of the magnetic field can be seen when the direction of the magnetic field is plotted on the orbit of MEX (Fig. 9c).

5. Discussion

This paper presents the first step to apply a QNH model to interpret new ion escape observations from the martian tail measured by Mars Express. This preliminary analysis leaves room for more detailed studies containing a larger data set and an improved QNH model. From the modelling point of view the future analysis should be based on a QNH model that (1) contains more ions in the simulation box in order to avoid artificial spatial and temporal fluctuations, (2) has a finer grid at the analysed spatial region, (3) has fine tuned values for the total ion production and ion emission rates, (4) contains a magnetic field model for the martian crustal magnetic field, and (5)

produces simulated IMA counts enabling a detailed comparison between the model and the IMA data. Especially, only after these improvements the QNH model can provide new information about the total ion outflow rates at Mars. Some degree of inaccuracy will, however, always remain when MEX ion data are analysed because no magnetic field data are available from Mars Express.

An interesting issue that has not been discussed so far concerns temporal variations. The QNH model never reaches a fully stationary stage, but always includes some fluctuations. For example, $n(O^+)$ shows a clear wavy ionotail boundary on the xz plane (Fig. 4f). When the solution of the presented run was studied by comparing solutions recorded at every 25-s time steps, clear "bursts," or ion "clouds" could be seen forming on the dayside near the planet and thereafter transferred to the nightside. The magnetic field does not either remain at a stationary stage and fluctuations both in the magnitude and in the direction of **B** exist (see, for example, Fig. 8g) can be found. When the properties of the magnetic field and plasma parameters were studied at a few points on the nightside by recording plasma and field parameters at every time step dt ($=0.04$ s) fluctuations with intervals of about 10 and 20 s can be identified by visual inspection (figures not shown). Although these variations may be artefacts, for example, from a too small number of particles used in the simulation, it is interesting to note that plasma and magnetic field fluctuations are recorded at Mars by MGS (see Espley et al., 2004) and MEX. One of the four individual detectors, Electron Spectrometer (ELS), of the ASPERA-3 instrument measures electrons with a good energy and temporal resolution (see Barabash et al., 2004, for the details of the ELS instrument). ELS has observed electron oscillations whose frequency peaks typically in the range of 0.01–0.02 Hz (Winningham et al., 2006). A study of the origin of the fluctuations and their role in the ion escape at Mars is, however, beyond the scope of the present study.

6. Summary

New observations of the escaping planetary ions at Mars from Mars Express are interpreted by a 3-D quasi-neutral hybrid (QNH) model. The model was found to produce high energy planetary ions in the hemisphere where the convective electric field accelerates the ions in agreement with ASPERA-3/Mars Express observations. The direction of the interplanetary magnetic field was derived from simultaneous Mars Global Surveyor measurements. The analysis indicates that combining a 3-D QNH model with Mars Express ion escape measurements and Mars Global Surveyor magnetic field measurements provides new possibilities to interpret ion escape data and to obtain new insight of the overall 3-D Mars–solar wind interaction.
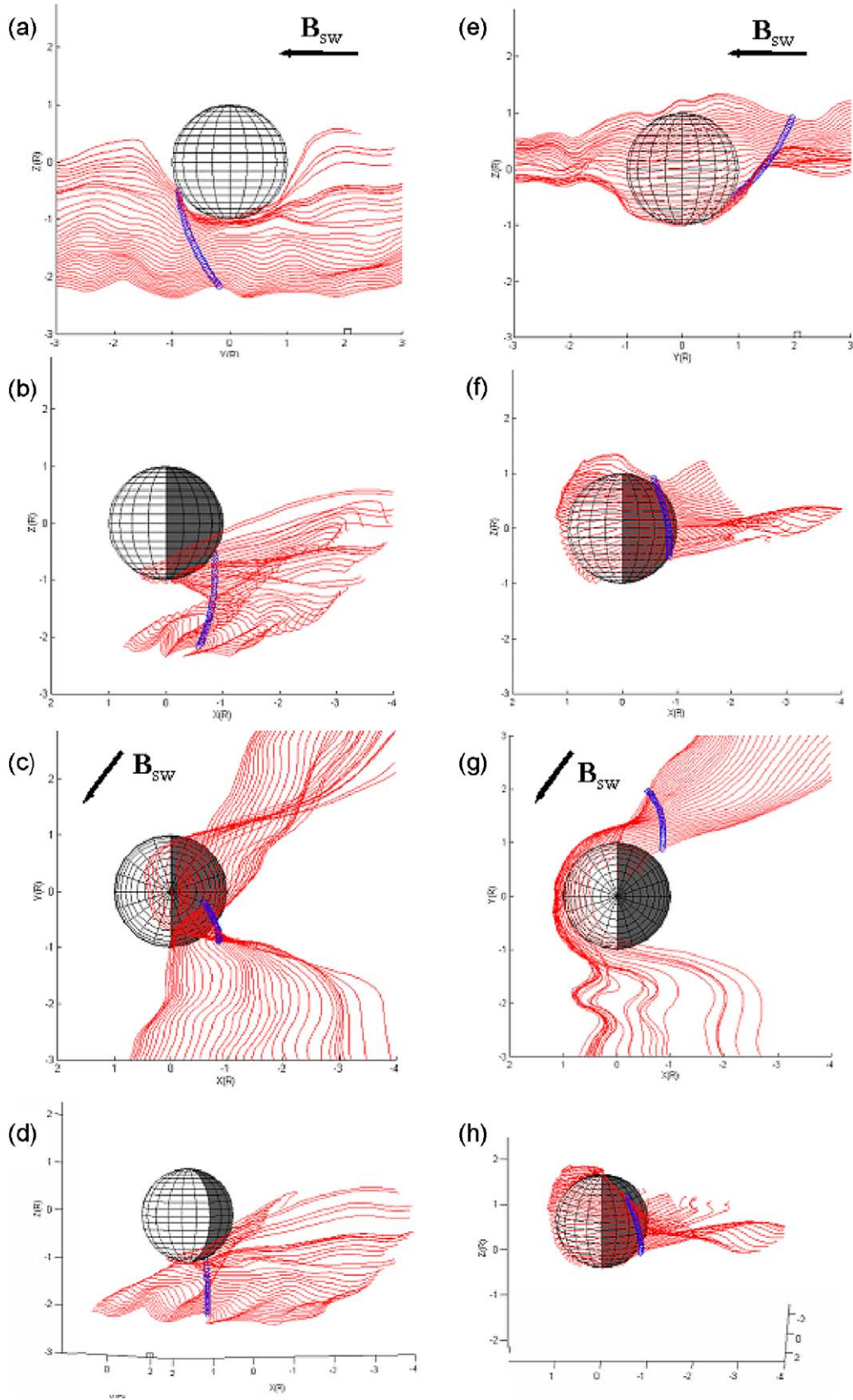
Acknowledgments

Fig. 8. (a–d) The magnetic field lines connecting to the orbit of MEX on June 27, 2004 at 03:00–03:35 UT from four view angles. The magnetic field line tracing was started from the positions along the orbit of MEX marked by blue circles. Note that the orbit of MEX seen in Fig. 2 is rotated around the x-axis until the IMF component perpendicular to x-axis, $[B_y, B_z] = [\cos(300°), \sin(300°)] \times 1.12$ nT $= [-0.866, 0.5] \times 1.12$ nT, pointed to the $-y$ direction. (e–h) The magnetic field lines if the IMF component perpendicular to the x-axis had been pointed to the $-y$ direction as seen from four view directions.
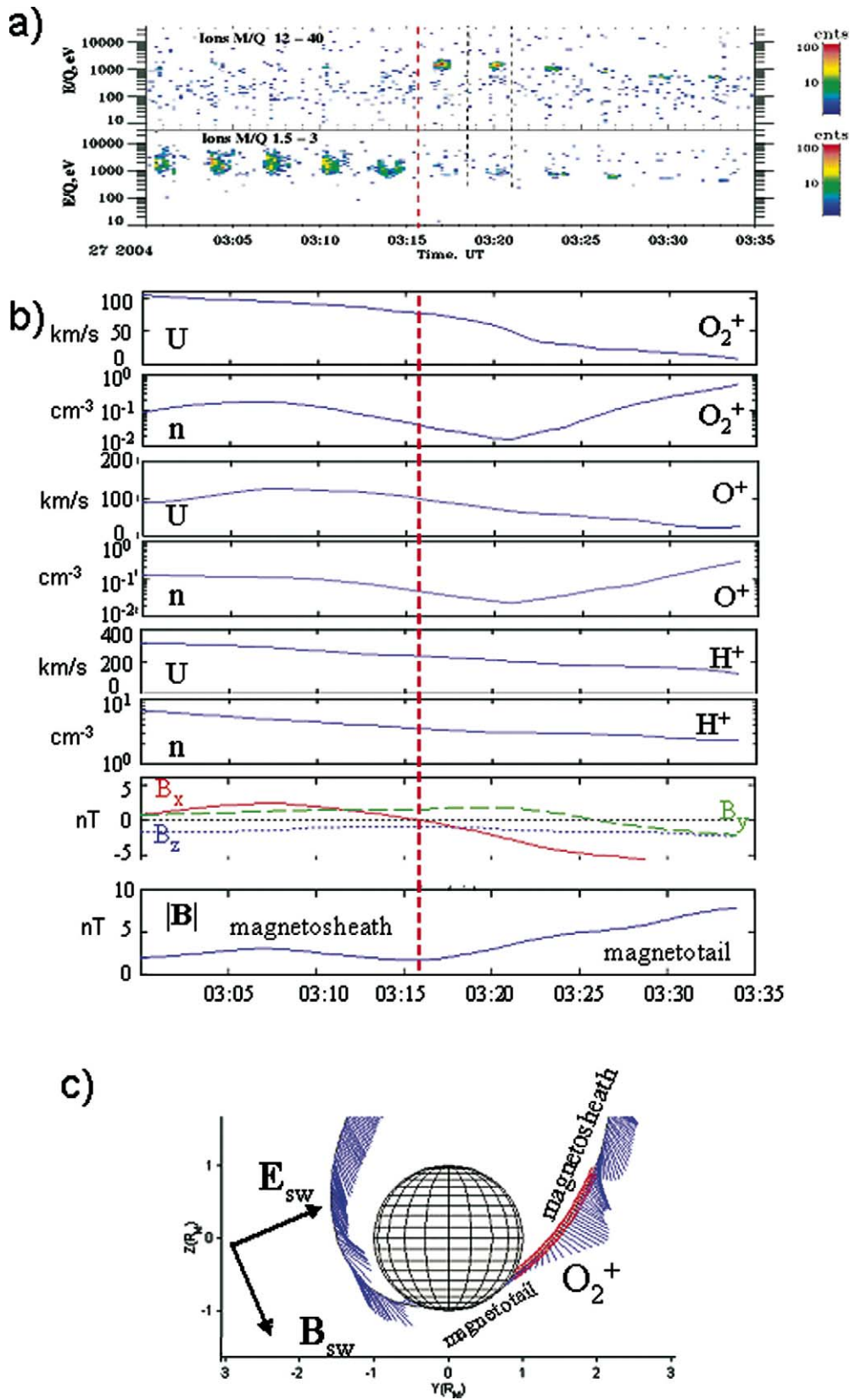
Fig. 9. A comparison between IMA observations and a hybrid model. (a) IMA heavy ion ($m/q = 12$–40 amu e^{-1}) and light ion ($m/q = 1.5$–3 amu e^{-1}) measurements from June 27, 2004 at 03:00–03:35 UT (the same data as shown in Fig. 1). (b) The bulk velocity (U [km s^{-1}]) and the plasma density (n [cm^{-3}] in log$_{10}$ scale) for O$_2^+$, O$^+$, and H$^+$ ions, and the magnetic field B_x [nT], B_y [nT], B_z [nT], and |**B**| [nT] along the orbit of MEX based on the hybrid model. The black dashed line in the magnetic field component panel gives the zero line. (c) The orbit of MEX on June 27, 2004. The red circles present the position of MEX at 03:00–03:35 UT and the blue vectors show unit magnetic field vectors plotted on the orbit of the spacecraft. The IMF clock angle is 300°.

institutes hosting these efforts. One of the authors (A. Fedorov) thanks M. Acuña and C. Mazelle for kind permission to use MGS data to estimate solar wind conditions.

References

Acuña, M.H., and 19 colleagues, 1998. Magnetic field and plasma observations at Mars: Initial results of the Mars Global Surveyor mission. Science 279, 1676–1680.

Barabash, S., Holmström, M., Lukyanov, A., Kallio, E., 2002. Energetic neutral atoms at Mars. IV. Imaging of planetary oxygen. J. Geophys. Res. 107 (A10), doi:10.1029/2001JA000326. 1280.

Barabash, S., and 47 colleagues, 2004. The analyser of space plasmas and energetic atoms (ASPERA-3) for the European Mars Express mission. In: Wilson, A. (Ed.), Mars Express: A European Mission to the Red Planet. ESA, ESTEC, Noordwijk, The Netherlands, pp. 121–139. ESA publication SP-1240.

Brecht, S.H., Ferrante, J.F., 1991. Global hybrid simulation of unmagnetised planets: Comparison of Venus and Mars. J. Geophys. Res. 96, 11209–11220.

Espley, J.R., Cloutier, P.A., Brain, D.A., Crider, D.H., Acuña, M.H., 2004. Observations of low-frequency magnetic oscillations in the martian magnetosheath, magnetic pileup region, and tail. J. Geophys. Res. 109, doi:10.1029/2003JA010193. A07213.

Fedorov, A., and 44 colleagues, 2006. Structure of the martian wake. Icarus 182, 329–336.

Kallio, E., 1996. An empirical model of the solar wind flow around Mars. J. Geophys. Res. 101, 11133–11147.

Kallio, E., Janhunen, P., 2002. Ion escape from Mars in a quasi-neutral hybrid model. J. Geophys. Res. 107 (A3), doi:10.1029/2001JA000090.

Lundin, R., Zakharov, A., Pellinen, R., Barabash, S.W., Borg, H., Dubinin, E.M., Hultqvist, B., Pissarenko, N., Liede, I., Koskinen, H., 1990. ASPERA/Phobos measurements of the ion outflow from the martian atmosphere. Geophys. Res. Lett. 17, 873–876.

Lundin, R., and 44 colleagues, 2004. Solar wind-induced atmospheric erosion at Mars: First results from ASPERA-3 on Mars Express. Science 305, 1933–1936.

Ma, Y., Nagy, A.F., Sokolov, I.V., Hansen, K.C., 2004. Three-dimensional, multispecies, high spatial resolution MHD studies of the solar wind interaction with Mars. J. Geophys. Res. 109, doi:10.1029/2003JA010367. A07211.

Shimazu, H., 1999. Three-dimensional hybrid simulation of magnetised plasma flow around an obstacle. Earth Planets Space 51, 383–393.

Slavin, J., Schwingenschuh, A.K., Riedler, W., Yeroshenko, Ye., 1991. The solar wind interaction with Mars: Mariner 4, Mars 2, Mars 3, Mars 5, and Phobos 2 observations of bow shock positions and shape. J. Geophys. Res. 96, 11235–11241.

Winningham, D., and 44 colleagues, 2006. Electron oscillations in the induced martian magnetosphere. Icarus 182, 360–370.